ISSN 1063-7745, Crystallography Reports, 2024, Vol. 69, No. 4, pp. 569–576. © Pleiades Publishing, Inc., 2024.

NANOMATERIALS AND CERAMICS

Microfluidic-Assisted Synthesis of Hybrid Carbonate Calcium Microparticles Modified by Silver Nanoparticles

A. V. Ermakov[a], S. V. Chapek[b], E. V. Lengert[a], P. V. Konarev[c], V. V. Volkov[c], M. A. Soldatov[b], and D. B. Trushina[a,c,*]

[a] *Institute of Molecular Theranostics, First Moscow State Medical University (Sechenov University), Moscow, 119991 Russia*

[b] *Smart Materials Research Institute, Southern Federal University, Rostov-on-Don, Russia*

[c] *Shubnikov Institute of Crystallography, Kurchatov Complex of Crystallography and Photonics, National Research Centre "Kurchatov Institute," Moscow, 119333 Russia*

**e-mail: trushina.d@mail.ru*

Received December 27, 2023; revised January 9, 2024; accepted January 9, 2024

Abstract—The development of advanced methods for the synthesis of nano- and microparticles for biomedical applications is of considerable interest. A method for synthesizing submicron silver-shelled calcium carbonate particles using a microfluidic chip designed to control the particle formation is proposed. Precise control of reaction parameters enables controlled formation of silver shell and calcium carbonate particles. The distribution of pores in the hybrid particles was analyzed using small-angle X-ray scattering, which gained insight into the complex structure of the pores. The results provide information on the particle morphology and may facilitate the development of new calcium carbonate-based materials for various applications.

DOI: 10.1134/S1063774524600546

INTRODUCTION

In recent years significant progress has been achieved in the development of the methodology of synthesizing materials designed for drug delivery systems [1–5]. The growing need in the production of multifunctional carriers for drug delivery is on the cutting edge of scientific achievements. These carriers require peculiar structural configurations, such as core–shell structures and multicomponent configurations. These particles can perform simultaneously several functions, including prolongation of blood circulation, enhancement of particle holding in pathologically changed vessels, and specific internalization [6–8]. These properties are necessary to provide efficient therapy even at the level of individual cells [9–11].

A promising strategy for improving synthesis procedures implies the use of microfluidic technologies, which open up new possibilities for the synthesis and analysis of nanostructured materials [12, 13]. The key advantage is the possibility of implementing unified reaction conditions, which is problematic in bulk processes. In addition, simultaneous in situ analysis can be performed using different methods.

The emergence of interdisciplinary technologies based on microfluidics has radically changed the concept of lab-on-a-chip devices, having provided a unique approach to the formation of nano- and microparticles [14–16]. Microfluidic chips make it possible to form homogeneous drops, maximally increasing the ratio of the surface area to the volume in which reaction occurs in order to increase the reaction kinetics efficiency. This design feature provides fast mass transfer in microreactors (drops), facilitating interaction between the reaction components [17].

Among the materials attracting much attention of the researchers engaged in the development of systems for encapsulation and delivery of biologically active substances, calcium carbonate ($CaCO_3$) can be noted. Its high potential can be implemented in various problems: from transdermal delivery to cancer therapy [18, 19]. The porous structure and excellent biocompatibility make calcium carbonate a promising carrier of theranostic agents. These properties are provided by the specificity of calcium carbonate synthesis, which implies aggregation of numerous nuclei, leading to the formation of a porous structure.

Calcium carbonate particles in the composition of vaterite polymorph, whose sizes varied from several hundred nanometers to several micrometers, demonstrated a high loading ability. They can incorporate high doses of medicines, retaining biocompatibility and facilitating safe long-term storage of loaded drugs [19, 20]. These properties, along with the small average size and spherical shape of particles, are decisive factors from the point of view of drug delivery. Promising characteristics and successful preclinical results

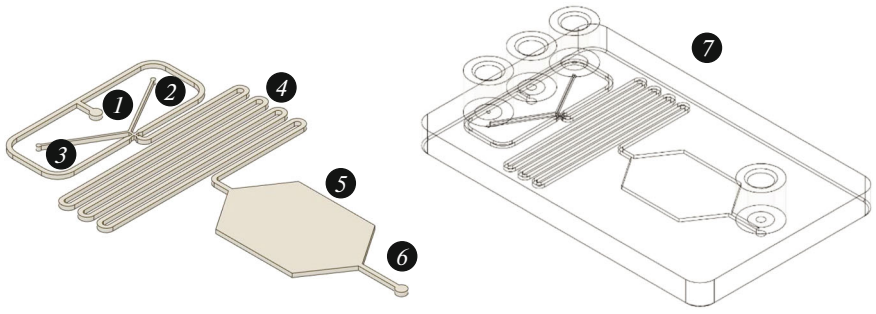

Fig. 1. Microfluidic device topology: (*1*) transport phase input, (*2*) agent 1, (*3*) agent 2, (*4*) reaction zone, (*5*) drop storage chamber, (*6*) output, and (*7*) general view.

of using calcium carbonate particles for drug delivery were demonstrated in different studies [21, 22]. Several key factors, such as the electrokinetic potential of particles, their loading ability, and biocompatibility, especially strongly affect the efficiency of calcium carbonate as a drug carrier [23].

The latest achievements in the field of microcarriers based on $CaCO_3$ opened up possibilities for developing systems for transdermal delivery of antimycotics [24], antimicrobial preparations [25, 26], multifunctional proteins [27], and enzymes [28] in many applications [2]. Along with the strategies of loading vaterite particles with functional compounds, the synthesis of core–shell structures is another promising field for development. Various microcarriers based on $CaCO_3$ have been created, including those using calcium carbonate as a functional core [29] or hollow capsules with a possibility of removing the core [30].

In this paper we present an approach using the potential of the drop method in a microfluidic 3D-printed device. Our main purpose was to apply this methodology to synthesize hybrid submicron vaterite particles with a silver shell: $CaCO_3$@Ag. The attention was focused on the estimation of the potential applicability of the obtained particles as drug carriers. To estimate in detail the validity of hybrid particles in this context, we thoroughly analyzed their properties, including the pore size, load ability, and antibacterial activity.

EXPERIMENTAL

Materials and agents. We used the following agents: calcium chloride ($CaCl_2$), sodium carbonate (Na_2CO_3), castor oil, ethylene glycol, bovine serum albumin (BSA, 66 kDa), silver nitrate ($AgNO_3$), tetramethylrhodamine (TRITC), hexane, isopropyl alcohol, ethanol production (Sigma-Aldrich, Germany), and 5% solution of glucose ($C_6H_{12}O_6$) (ThermoFisher Scientific, USA). The experiments were performed using deionized water with a resistivity more time 18.2 MΩ/cm, purified on a Milli-Q Plus system (Millipore, USA).

Design and fabrication of microfluidic device. The design and production of 3D-printed microfluidic chips were described in [31]. The device topology was designed using a computer-aided (CAD) system Fusion 360 (Autodesk, USA) and adapted for the synthesis of calcium carbonate particles by forming drops of aqueous salt solutions in castor oil [32]. The microfluidic device topology is presented in Fig. 1. Microreactors are formed at the interface of the two-phase system: castor oil (input 1) and aqueous solutions of two reagents (inputs 2, 3). A size of 200 × 200 μm was set for the main input channels, and 400 × 200 μm channels were used for the reaction and storage zones.

A 3D printer MAX UV (Asiga, Sydney, Australia) was used for printing a microfluidic device according to the DLP (Digital Light Processing) technology. The protocols published in [33] were adapted to improve printing and detach the model from the platform after the printing. Photopolymer resin Nano Clear (FunToDo, the Netherlands) was applied at a temperature of 50°C during the layer formation. Immediately after printing the microfluidic device was washed in isopropyl alcohol. In the last stage the chips were processed for 5 min using an UV lamp (Flash DR-301C, Asiga, Sydney, Australia).

Synthesis of $CaCO_3$ and $CaCO_3$@Ag in the microfluidic device. To study the synthesis of calcium carbonate in single drops, we performed experiments with the microfluidic device (Fig. 2). To crystallize calcium carbonate, small amounts of equimolar 1 M solutions of calcium chloride and sodium carbonate were fed through the two inputs of the microfluidic device with a flow velocity of 0.3 mL/h. The salt solutions were mixed in two experimental modes: (i) individual use in the form of pure solutions and (ii) joint use with added 0.1 M $AgNO_3$ and excess amount of NH_4OH. Drops were formed using a system for water flow focusing by castor oil with a flow velocity of 0.5 mL/h. Then the formed particles, jointly with $Ag(NH_3)_2OH$, were treated by a 5% glucose solution with simultaneous heating of the entire chip to 40°C. The reaction products were collected at the chip output, rapidly transferred to a 2-mL Eppendorf tube, and subjected to

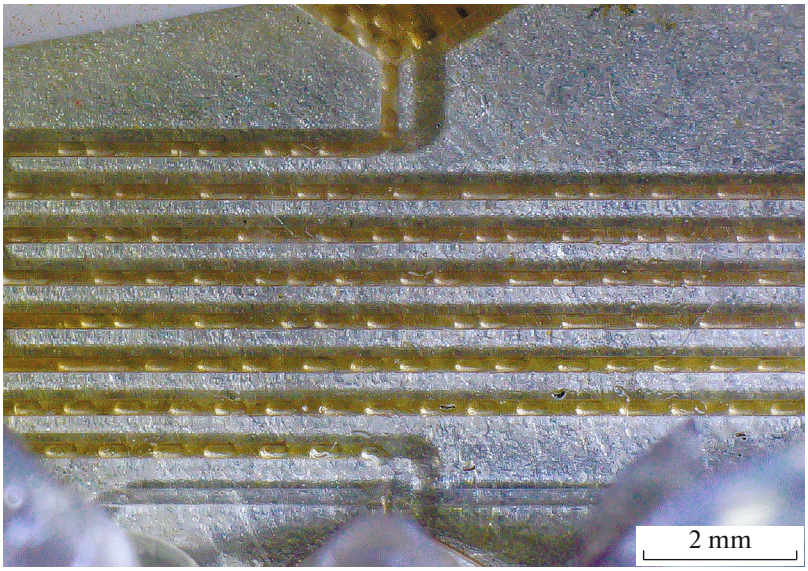

Fig. 2. Micrograph of the microfluidic chip plane during formation of $CaCl_2/Na_2CO_3$ drops in castor oil with addition of 0.1 M $AgNO_3$ and excess amount of NH_4OH, with subsequent washing in 5% glucose ($C_6H_{12}O_6$) solution.

several cycles of washing in hexane and ethanol. Dry particle powders were obtained after washing in ethanol and drying in air.

In addition, we performed control experiments, in which calcium carbonate was deposited in the bulk phase. The control $CaCO_3$ sample was formed using the technique studied in detail in [34]. A modified protocol, implying synthesis of spherical $CaCO_3$ microparticles with a porous structure was applied to this end. Specifically, 0.5 mL of 0.5 M $CaCl_2$ solution and 0.5 mL of 0.5 M Na_2CO_3 solution were introduced into a viscous medium (polyatomic alcohol) containing 4 mL of ethylene glycol, placed in a 25-mL laboratory glass vessel. Then the mixture was stirred using a standard 1-cm long magnetic anchor on a magnetic agitator with a rotational speed of 500 rpm. After 2-h stirring the obtained suspension was separated by centrifugation and washed two times with water and alcohol.

Loading of $CaCO_3$ particles by a model compound. To synthesize the model conjugate, a TRITC solution (1 mg) was carefully dissolved in 5 mL of ethanol. The thus obtained TRITC solution was added to a BSA solution (20 mL, 4 mg/mL, carbonate-bicarbonate buffer, pH 8.5), and the mixture was continuously stirred for 12 h at 4°C. Then the TRITC–BSA solution was subjected to dialysis against deionized water for four days to remove residual agents. Loading of $CaCO_3$ microparticles was implemented by freezing the suspension in the presence of the target compound according to the technique described in [11]. To this end, 2 mL of the TRITC–BSA solution were added to 10 mg of $CaCO_3$ particles, and the mixture was placed in a microcentrifuge test tube and incubated in a freezing chamber at −17°C for 2 h, with slow stirring. Then the samples were defrosted at room temperature, carefully washed, and dried in a drying box. The freezing/defrosting cycle was repeated three times. Loading was also performed by coprecipitation; in this case, the encapsulated material was introduced during the synthesis of calcium carbonate particles. This loading technique was implemented either in the microfluidic chip or in the bulk phase.

The antimicrobial activity of $CaCO_3$@Ag particles against the *Escherichia coli* strain was estimated using the modified method for determining the minimum inhibiting concentration. To provide statistical significance, experiments were repeated three times. The *E. coli* strain used in our study was grown and supplied by the Scientific Research Institute of Traumatology, Orthopedics, and Neurosurgery (Saratov, Russia). In each experiment 300 mL of suspensions containing microorganisms in a concentration of 3×10^5 cells/mL were mixed with suspensions having different concentrations: from 1 to 15 studied particles per bacterial cell. The mixture was incubated for 60 min. After the incubation, each light-processed suspension (100 mL in volume) was inoculated onto the surface of a nutrient medium (agar), obtained from 20 mL of sterile 1.5% agar medium solidified in Petri dishes. Then the Petri dishes were incubated at 37°C for 24 h to provide growth of individual bacterial colonies on the solid-medium surface. The initial cell concentration in suspensions was corrected to exclude continuous growth. Bacteria samples cultured under the same conditions without adding a suspension of studied particles were used for negative control. Alternatively, to verify the results, the antibacterial activity of hybrid vaterite par-

ticles with silver shells was measured using the standard method of minimum inhibiting concentration.

Physico–chemical methods of study. The size, shape, and surface morphology of the particles were analyzed on a scanning electron microscope (SEM) Jeol 7401F (JEOL, Akishima, Japan). To this end, an aqueous suspension of calcium carbonate particles was deposited on a silicon plate; SEM images were obtained using the lower secondary-electron detector at an accelerating voltage of 1 kV and a working distance of 8–9 mm.

To determine the concentration of the model compound in the samples, we performed spectroscopic measurements using a microplate reader Infinite 200 PRO (Tecan, Switzerland). The fluorescence intensity was determined quantitatively and compared with the previously plotted calibration line in order to calculate the concentration. The particle load (in wt percent) was calculated as the mass ratio of the incorporated material to the particles. The hydrodynamic particle size in the aqueous suspension was found by dynamic light scattering (DLS) using an automatic analyzer ZetasizerNano-ZS (Malvern, UK).

Small-angle X-ray scattering (SAXS) measurements were performed on an automatic diffractometer AMUR-K (Institute of Crystallography, Moscow, Russia). This diffractometer is equipped with a Kratky collimation system and a single-axis position-sensitive gas detector OD-3M. SAXS measurements were carried out at a fixed wavelength $\lambda = 0.1542$ nm, which provided a momentum transfer range from 0.11 to 10.0 nm^{-1}. Samples of $CaCO_3$ powders were measured in a specially designed cuvette with 15-μm-thick mylar windows, placed in a vacuum chamber. The sample–detector distance was 700 mm, and the exposure time was 10 min. Collimation distortions were corrected according to standard techniques, and the scattering signal from an empty cuvette was subtracted from the sample scattering intensity using the PRIMUS program from the ATSAS software package. To calculate the size distribution of pores/particles on the assumption of their spherical shape, we used a parametric simulation of the size distribution, consisting of a superposition of smooth analytical Schulz distribution functions (MIXTURE program from the ATSAS package). The nonlinear minimization method was applied to determine the positions, half-widths, and relative contributions of distribution functions. The optimal starting fittings for the MIXTURE program were estimated by two alternative approaches: (i) linear least-squares method using the indirect Fourier transform with Tikhonov regularization of the solution to search directly for the size distribution of pores/particles (GNOM program from the ATSAS package) and (ii) the technique based on a histogram of an arbitrary shape to search directly for the size distribution of pores/particles (VOLDIS program).

RESULTS AND DISCUSSION

Based on the data in the literature on the possibility of synthesizing calcium carbonate particles using a microfluidic chip, the chip parameters were optimized for carrying out the synthesis [35, 36]. Controlled growth of calcium carbonate particles can be implemented by mixing calcium chloride and sodium carbonate salts in small limited drop volumes, thus limiting the resource available for crystallization. Combination of $AgNO_3$ and NH_4OH in coprecipitation leads to the formation of the $Ag(NH_3)_2NO_3$ complex, which penetrates the calcium carbonate particles formed during crystallization:

$$AgNO_3 + 2NH_4OH \rightarrow [Ag(NH_3)_2]NO_3 + H_2O. \quad (1)$$

Glucose was used for further reduction of silver, especially on the surface of particles and in the immediate vicinity of pore walls. This additional stage facilitates reduction and promotes incorporation of Ag nanoparticles (NPs) into calcium carbonate particles:

$$6[Ag(NH_3)_2]NO_3 + C_6H_{12}O_6 \rightarrow C_6H_8O_6 + 6Ag\downarrow + 12NH_3 + 6HNO_3. \quad (2)$$

The SEM images in Fig. 3 visualize the carbonate particles obtained during microfluidic synthesis and synthesis in a large-volume flask using ethylene glycol. The SEM and DLS data (Fig. 4) show that the mean size of the particles synthesized in the chip is ~650 nm, whereas the bulk synthesis method made it possible to obtain particles with a minimum size of ~900 nm. In addition, the SEM images clearly demonstrate a change in the particle morphology after the silver reduction. We performed an additional SEM study of the sample in the backscattered-electron mode to detect the presence of heavy elements (in particular, silver) on the surface of calcium carbonate particles. Figure 3c presents a unified SEM image, where bright areas correspond to the areas demonstrating contrast characteristics in the backscattered-electron mode.

According to [37, 38], incorporation of silver and gold NPs leads to efficient enhancement of the Raman scattering signal. Thus, using Raman spectroscopy, one can detect substances present in the medium in ultralow concentrations. The combination of therapeutic (antibacterial) property of Ag NP with the possibility of their application for diagnostic purposes (detection of very small amounts of various chemical agents) opens prospects for designing a multifunctional carrier for theranostics. The use of the core–shell system with Ag NPs in the shell will make it possible both to enhance the inhibiting action on microorganisms and to increase the diagnostics efficiency because of the larger area of interaction with microorganisms and analyzed environment.

The samples obtained were analyzed by the SAXS method (Fig. 5). Proceeding from the assumption of spherically shaped pores, submicron vaterite particles,

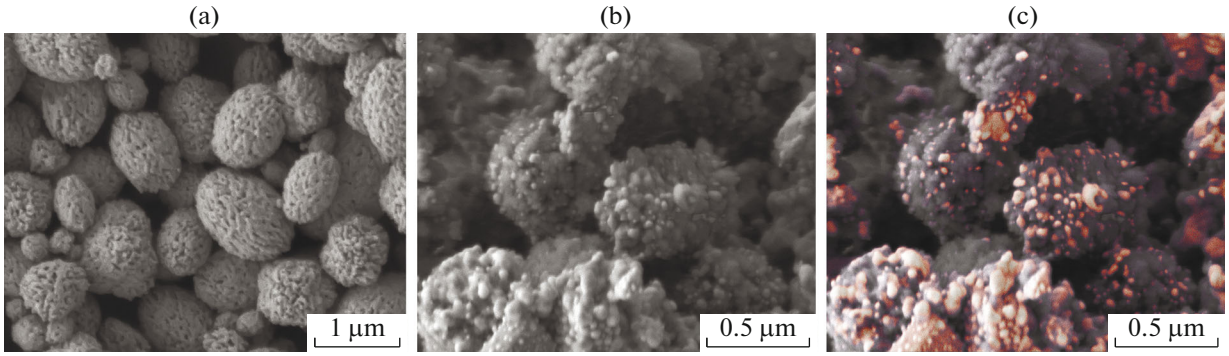

Fig. 3. SEM images of the (a) $CaCO_3$ particles synthesized in the bulk phase using ethylene glycol and (b, c) hybrid $CaCO_3$@Ag particles, synthesized by the drop method using a microfluidic device in the standard mode (b) and in combination with the back-scattered-electron mode (c).

synthesized under bulk conditions, demonstrated a distribution of pore radii in the range from 3 to 40 nm. These particles are characterized by the presence of pores with sizes both of few nanometers and of several ten nanometers, with the maximum radius in the range of 15–25 nm [23, 38]. The interpretation of the SAXS data on the $CaCO_3$@Ag sample is ambiguous due to the presence of scattering inhomogeneities of two types: pores and Ag NPs themselves. The scattering curve intensity and shape are independent of the contrast sign, in correspondence with the Babinet's principle [39]. Thus, it is difficult to distinguish between the scattering from pores (with a negative contrast relative to the matrix density) and from NPs (having a positive contrast). The formation and growth of NPs in a small volume in the presence of calcium carbonate may lead to different results. $CaCO_3$ can play the role of a matrix for the growth of Ag NPs, thus increasing the scattering intensity in the range of sizes corresponding to the pores. However, judging from the distribution curve $Dv(r)$ in Fig. 5b, one can conclude that there occurred another mechanism. Likely, the increase in the tail of size distribution function in the range of radii from 25 to 40 nm is caused by the formation of silver aggregates on the surface of $CaCO_3$ particles. The contribution of Ag NPs in this part of the curve increases, because they have a tendency to precipitate on irregularities of the $CaCO_3$ particle surface. In the range of sizes from 5 to 25 nm the distribution becomes more uniform, because the isolated peaks at 7.5 and 16 nm are smoothed out. This may be related to the incorporation of Ag NPs into the newly formed pores in $CaCO_3$. In contrast, the distribution curve for $CaCO_3$@Ag is smoother, without any pronounced peaks, as in the case where Ag NPs grow in the presence of a nanostructured surface [41]. The silver mirror reaction (2) leads to the formation of polydisperse Ag NPs with a relatively uniform size distribution, which is consistent with the SEM data (Fig. 3). It was shown in [42] that the formation of a shell from NPs on the surface of calcium carbonate particles by the solvent freezing method does not affect their polymorphic composition and does not cause any recrystallization of vaterite particles and increase in the calcite phase content. Due to this circumstance, the porosity of particles is retained, which is favorable for their loading ability.

Loading efficiency. The loading procedure included cyclic freezing of the particle suspension with immersion into the TRITC–BSA solution. Then the particles were separated from the solution by centrifugation, and the liquid obtained was collected for spectrophotometric estimation of the model substance concentration. An analysis of the experimental data revealed significant differences in the loading ability of the hybrid vaterite particles ($CaCO_3$@Ag) synthesized in the microfluidic chip and the control-group particles, obtained by bulk synthesis. In particular, the vaterite particles synthesized using the microfluidic device demonstrated a loading ability of ~11 wt %, whereas the bulk vaterite particles had a loading ability

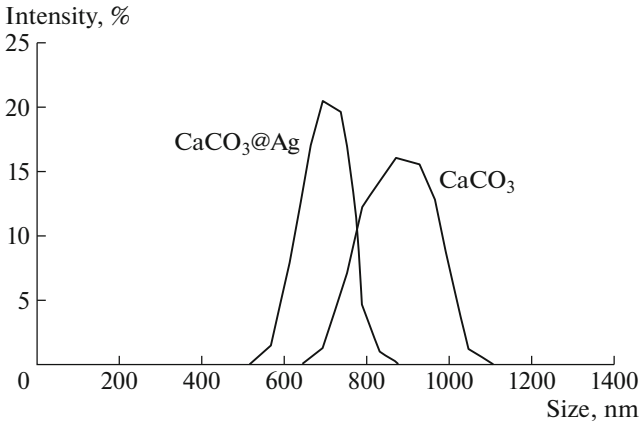

Fig. 4. DLS data on the distribution of the $CaCO_3$ particles synthesized in the bulk phase using ethylene glycol and the hybrid $CaCO_3$@Ag particles synthesized by the drop method using a microfluidic device.

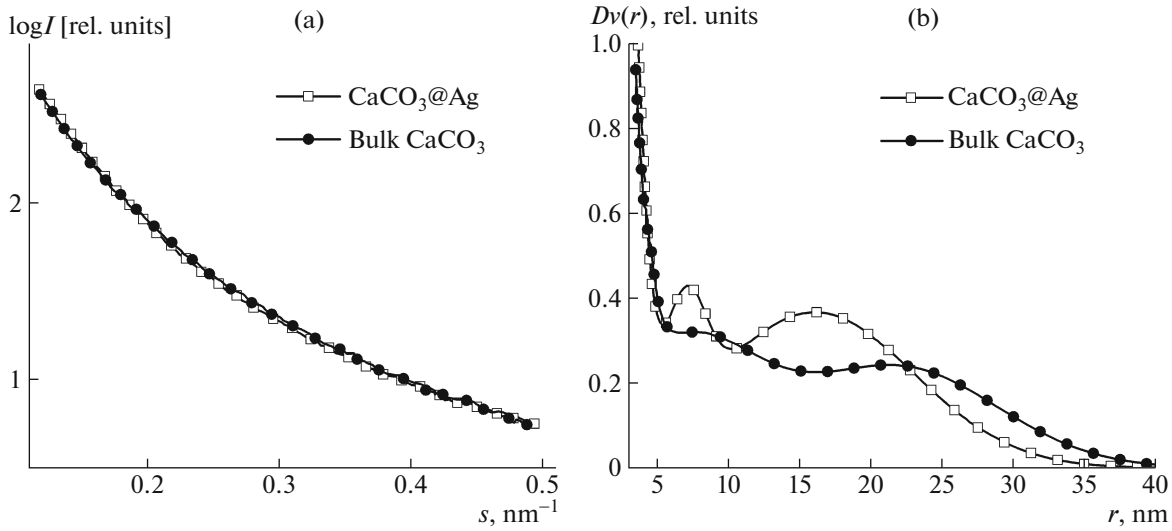

Fig. 5. (a) Experimental SAXS curves and (b) distribution functions $Dv(r)$ for the $CaCO_3$ particles synthesized in the bulk phase and in the microfluidic chip with formation of Ag NPs.

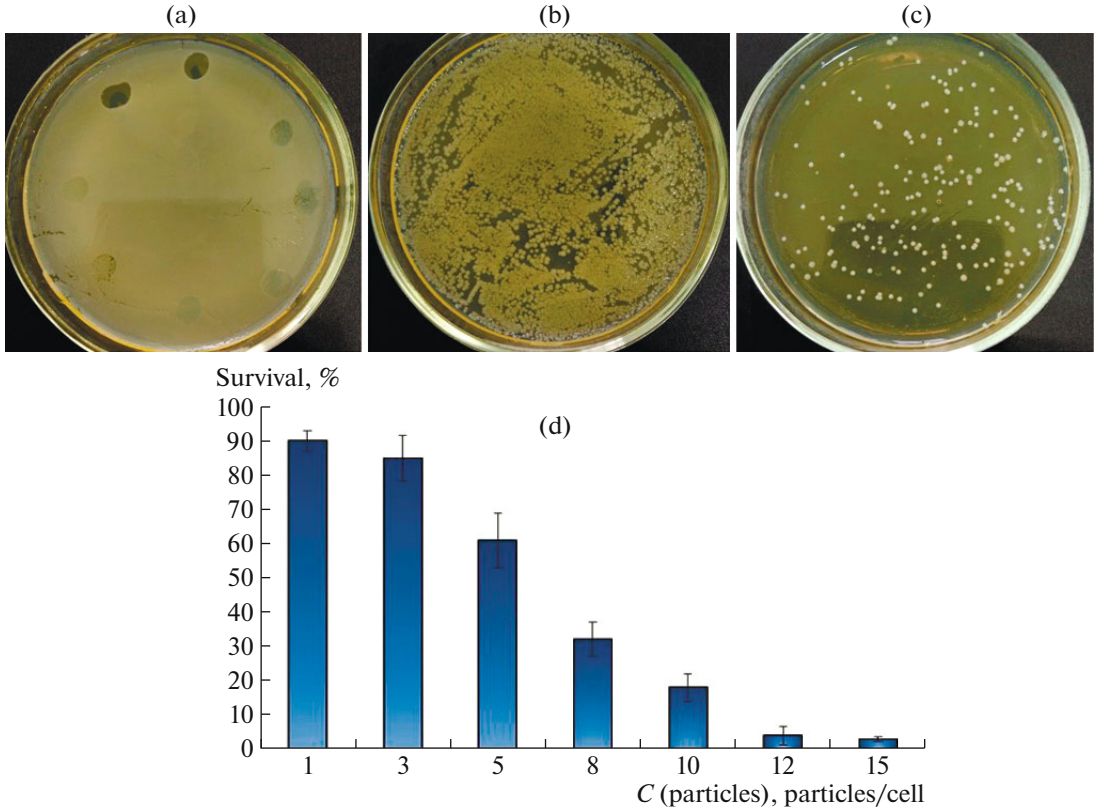

Fig. 6. Antibacterial activity of hybrid vaterite $CaCO_3$@Ag particles according to the (a) standard method of minimum inhibiting concentration and (b–d) the modified method: (b) control, (c) particles with a concentration of 10 particles per cell, and (d) bacterial cell vitality in dependence of the number of hybrid $CaCO_3$@Ag particles added to the cultural medium.

of only 9 wt %. This difference in the loading ability is likely due to the fact that the particles obtained using with the aid of the microfluidic device have larger surface area, increased porosity, and smaller size. These characteristics facilitate the enhancement of interaction and absorption for the TRITC–BSA conjugate. These results indicate advantages of the microfluidic device for the synthesis of particles with a high loading ability.

Antibacterial properties of $CaCO_3$@Ag. The antibacterial properties of silver nanoparticles are widely

known. One of the mechanisms of antibacterial activity of Ag NPs is their ability to release (when contacting a bacterial cell) positively charged silver ions (Ag^+), which have a high reactivity and violate the integrity of the cell wall of bacteria. Hybrid $CaCO_3$@Ag particles should also possess antibacterial activity, despite the likely less efficient interaction of Ag NPs in comparison with highly dispersed suspensions. Silver ions can penetrate cellular membranes, which leads to violation of the main functions of cellular components, including proteins and nucleic acids. This violation suppresses the most important cellular processes and impedes the growth of bacteria, which finally leads to their annihilation. In addition, the specific physicochemical properties of Ag NPs facilitate to a great extent their antibacterial activity.

The results obtained by the method of minimum inhibiting concentration revealed that a suspension of hybrid vaterite particles with a concentration exceeding 15 particles per bacterial cell completely suppresses the growth of bacteria (Fig. 6a). In addition, a modified estimation method was applied, the essence of which is incubation of a suspension of bacteria and particles, with subsequent deposition of the incubated suspension on the surface of a nutrient medium (agar) and analysis of the number of colonies. The bacterial suspension concentration was chosen thoroughly to exclude continuous growth (Figs. 6b, 6c). Thus, the mean number of colonies in the absence of $CaCO_3$@Ag particles was taken as corresponding to the 100% survival. The plot in Fig. 6d illustrates the relationship between the bacteria survival and particle concentration. The estimation based on this plot made it possible to determine the minimum inhibiting concentration, which falls in the range of 12–15 particles per cell. These results are consistent with the data obtained by the standard approach, which is generally used in such studies.

CONCLUSIONS

A new approach to the synthesis of hybrid calcium carbonate particles, modified by Ag NPs with the aid of a microfluidic device, was presented. The synthesized particles were characterized by the SEM and DLS methods, which showed successful formation of these particles; their difference in morphology; and the presence of Ag NPs, distributed over the vaterite surface. These results demonstrate a fundamental possibility of forming hybrid functional submicron $CaCO_3$@Ag particles during crystallization in microvolumes and open up new possibilities for controlling the parameters of such systems. The additional advantages of the developed approach are the scalability and reproducibility of the synthesis. The results showed that the particles synthesized in microvolumes exhibit a significant increase in the loading ability: about 11 wt % versus 9 wt % for the control sample. The analysis of the SAXS data revealed a significant fraction of pores with sizes ranging from 3 to 40 nm in the obtained particles, which indicates their potential as high-efficiency carriers for different applications, especially in antibacterial therapy. Hybrid $CaCO_3$@Ag particles, synthesized using a microfluidic device, exhibited high activity against gram-negative *E. coli* bacteria with an inhibiting concentration of 12–15 particles per cell. These results are important for drug delivery applications and open up possibilities for further research in the field of biomedical nanotechnologies.

ACKNOWLEDGMENTS

We are grateful to V. V. Artemov for the SEM study of the samples.

FUNDING

This work was supported by the Ministry of Science and Higher Education of the Russian Federation (Agreement no. 075-15-2021-1363, Contract No. 210EP on November 29, 2021).

ETHICS APPROVAL AND CONSENT TO PARTICIPATE

This work does not contain any studies involving human and animal subjects.

CONFLICT OF INTEREST

The authors of this work declare that they have no conflicts of interest.

REFERENCES

1. D. Yang, K. Gao, Y. Bai, et al., Int. J. Biol. Macromol. **182**, 639 (2021). https://doi.org/10.1016/j.ijbiomac.2021.04.057
2. R. A. Verkhovskii, A. N. Ivanov, E. Lengert, et al., Pharmaceutics **15** (5), 1566 (2023). https://doi.org/10.3390/pharmaceutics15051566
3. W. Song, Y. Zhang, D.-G. Yu, et al., Biomacromolecules **22** (2), 732 (2021). https://doi.org/10.1021/acs.biomac.0c01520
4. E. V. Lengert, D. B. Trushina, M. Soldatov, and A. V. Ermakov, Pharmaceutics **14** (1), 139 (2022). https://doi.org/10.3390/pharmaceutics14010139
5. Y. Huang, L. Cao, B. V. Parakhonskiy, and A. G. Skirtach, Pharmaceutics **14** (5), 909 (2022). https://doi.org/10.3390/pharmaceutics14050909
6. P. Trucillo, Processes **9** (3), 470 (2021). https://doi.org/10.3390/pr9030470
7. X. Zhao, D. Wu, X. Ma, et al., Biomed. Pharmacother. **128**, 110237 (2020). https://doi.org/10.1016/j.biopha.2020.110237

8. J. A. Finbloom, F. Sousa, M. M. Stevens, and T. A. Desai, Adv. Drug Deliv. Rev. **167**, 89 (2020). https://doi.org/10.1016/j.addr.2020.06.007

9. D. Turiel-Fernández, L. Gutiérrez-Romero, M. Corte-Rodriguez, et al., Anal. Chim. Acta **1159**, 338356 (2021). https://doi.org/10.1016/j.aca.2021.338356

10. J. Tu and A. C. H. Yu, BME Front. **2022** (2022). https://doi.org/10.34133/2022/9807347

11. M. V. Novoselova, S. V. German, T. O. Abakumova, et al., Colloids Surf. B **200**, 111576 (2021). https://doi.org/10.1016/j.colsurfb.2021.111576

12. C.-T. Kung, H. Gao, C.-Y. Lee, et al., Chem. Eng. J. **399**, 125748 (2020). https://doi.org/10.1016/j.cej.2020.125748

13. Z. Ma, B. Li, J. Peng, and D. Gao, Pharmaceutics **14** (2), 434 (2022). https://doi.org/10.3390/pharmaceutics14020434

14. Y. Liu, G. Yang, Y. Hui, et al., Small **18** (36), (2022). https://doi.org/10.1002/smll.202106580

15. K. S. Huang, C. H. Yang, Y. C. Wang, et al., Pharmaceutics **11** (5), 212 (2019). https://doi.org/10.3390/pharmaceutics11050212

16. Y. Huang, C. Liu, Q. Feng, et al., Nanoscale Horizons **8** (12), 1610 (2023). https://doi.org/10.1039/D3NH00217A

17. N. Hao, Y. Nie, and J. X. J. Zhang, Biomater. Sci. **7** (6), 2218 (2019). https://doi.org/10.1039/C9BM00238C

18. Y. Svenskaya and T. Pallaeva, Pharmaceutics **15** (11), 2574 (2023). https://doi.org/10.3390/pharmaceutics15112574

19. S. Maleki Dizaj, S. Sharifi, E. Ahmadian, et al., Expert Opin. Drug Deliv. **16** (4), 331 (2019). https://doi.org/10.1080/17425247.2019.1587408

20. P. Zhao, Y. Tian, J. You, et al., Bioengineering **9** (11), 691 (2022). https://doi.org/10.3390/bioengineering9110691

21. S. Westrøm, T. B. Bønsdorff, Ø. S. Bruland, and R. H. Larsen, Transl. Oncol. **11** (2), 259 (2018). https://doi.org/10.1016/j.tranon.2017.12.011

22. R. G. Li, K. Lindland, T. B. Bønsdorff, et al., Materials (Basel) **14** (23), 7130 (2021). https://doi.org/10.3390/ma14237130

23. N. Feoktistova, J. Rose, V. Z. Prokopović, et al., Langmuir **32** (17), 4229 (2016). https://doi.org/10.1021/acs.langmuir.6b00717

24. Y. I. Svenskaya, E. V. Lengert, Y. V. Tarakanchikova, et al., J. Mater. Chem. B **11** (17), 3860 (2023). https://doi.org/10.1039/D2TB02779H

25. A. M. Ferreira, A. S. Vikulina, and D. Volodkin, J. Control. Release **328**, 470 (2020). https://doi.org/10.1016/j.jconrel.2020.08.061

26. E. V. Lengert, A. A. Savkina, A. V. Ermakov, et al., Mater. Sci. Eng. C **126**, 112144 (2021). https://doi.org/10.1016/j.msec.2021.112144

27. M. V. Kiryukhin, S. H. Lim, H. H. Lau, et al., J. Colloid Interface Sci. **594**, 362 (2021). https://doi.org/10.1016/j.jcis.2021.03.059

28. A. S. Vikulina, N. A. Feoktistova, N. G. Balabushevich, et al., Phys. Chem. Chem. Phys. **20** (13), 8822 (2018). https://doi.org/10.1039/C7CP07836F

29. R. Jenjob, T. Phakkeeree, and D. Crespy, Biomater. Sci. **8** (10), 2756 (2020). https://doi.org/10.1039/C9BM01872G

30. B. G. De Geest, S. De Koker, G. B. Sukhorukov, et al., Soft Matter **5** (2), 282 (2009). https://doi.org/10.1039/B808262F

31. L. Garcia, G. Kerns, K. O'Reilley, et al., Micromachines **13** (1), 28 (2021). https://doi.org/10.3390/mi13010028

32. A. V. Ermakov, S. V. Chapek, E. V. Lengert, et al., Micromachines **15** (1), 16 (2023). https://doi.org/10.3390/mi15010016

33. V. V. Shapovalov, S. V. Chapek, A. A. Tereshchenko, et al., Micro Nano Eng. **20**, 100224 (2023). https://doi.org/10.1016/j.mne.2023.100224

34. G. B. Sukhorukov, D. V. Volodkin, A. M. Günther, et al., J. Mater. Chem. **14** (14), 2073 (2004). https://doi.org/10.1039/B402617A

35. A. Yashina, F. Meldrum, and A. DeMello, Biomicrofluidics **6** (2), 022001 (2012). https://doi.org/10.1063/1.3683162

36. H. Witt, N. Yandrapalli, M. Sari, et al., Langmuir **36** (44), 13244 (2020). https://doi.org/10.1021/acs.langmuir.0c02175

37. P. Tan, H. Li, J. Wang, and S. C. B. Gopinath, Biotechnol. Appl. Biochem. bab.2045 (2020). https://doi.org/10.1002/bab.2045

38. J. Horne, C. De Bleye, P. Lebrun, et al., J. Pharm. Biomed. Anal. **233**, 115475 (2023). https://doi.org/10.1016/j.jpba.2023.115475

39. I. Marchenko, T. Borodina, D. Trushina, et al., J. Microencapsul. **35** (7–8), 657 (2018). https://doi.org/10.1080/02652048.2019.1571642

40. L. A. Feigin and D. I. Svergun, *Structure Analysis by Small-Angle X-Ray and Neutron Scattering*, Ed. by G. W. Taylor (Springer, New York, 1987). https://doi.org/10.1007/978-1-4757-6624-0

41. T. V. Bukreeva, I. V. Marchenko, B. V. Parakhonskiy, and Y. V. Grigor'ev, Colloid J. **71** (5), 596 (2009). https://doi.org/10.1134/S1061933X09050032

42. A. V. Mikheev, T. N. Pallaeva, I. A. Burmistrov, et al., Cryst. Growth Des. **23** (1), 96 (2023). https://doi.org/10.1021/acs.cgd.2c00796

Translated by Yu. Sin'kov

Publisher's Note. Pleiades Publishing remains neutral with regard to jurisdictional claims in published maps and institutional affiliations.

AI tools may have been used in the translation or editing of this article.